Modelling Highly Skewed Chromatographic Response Curves

A model is presented in which damaged pores are distributed throughout a network of undamaged pores within a spherical particle. The differential equations are solved according to the numerical procedure of Haynes, Jr. (1975). The model is intended to simulate more highly skewed chromatographic response curves than the two-zone model recently proposed by Chou and Hegedus (1978).

Pulse chromatographic measurements in fresh NaMgA zeolites using i-butane as a tracer which only enters the macropores yield response curves with relatively low skew, which are readily fitted by a system of equations accounting for diffusion in a monodisperse pore system. For hydrothermally treated zeolites effective diffusivities and Henry constants are considerably lower and the skew higher than in fresh samples.

Curve fitting with the model proposed below is quite satisfactory, and the characteristic parameters determined are approximately constant at the flowrates studied. Application of the model should not be restricted to hydrothermally treated zeolites, but may be extended to catalysts or adsorbents with macroporous structures damaged by other forms of ageing.

D. GELBIN and H.-J. WOLFF

Central Institute of Physical Chemistry, Academy of Sciences of the German Democratic Republic, Berlin, East Germany

S. FRIEDRICH

Department of Chemistry, Karl-Marx University, Leipzig, East Germany

SCOPE

Evaluating parameters by the method of moments is a rapid and widely used procedure since the work of Kubin (1965). However, the moments method makes use of integrated functions of a response curve, and is therefore not model discriminatory, since various forms of a response curve can lead to the same lower-order moments. It is thus advisable to calculate sample response curves in the time domain with the parameter values determined by the moments method.

Our estimates show that for highly skewed pulse chromatographic response curves with hydrothermally treated zeolites satisfactory agreement could be expected neither with the common macropore model nor with the Chou and Hegedus (1978) two-zone model for spent catalysts, which assumes blockage at the outer shell of the pellet. The purpose of this work is to present and test a model for calculating highly skewed response curves on the basis of effective parameters determined from the first and second experimental moments.

It will be asumed that the monodisperse macroporous system disintegrates into a bidisperse system in the course of ageing. The undamaged pores act as transport pores and are assigned the Henry constant measured in the fresh sample. The damaged pores are distributed along the transport pores in the same manner as the micropores in the model of Ruckenstein et al (1971). Contrary to the common interpretation of the bidisperse model, the transport pores have the higher adsorption capacity. The remaining model parameters are determined by curve fitting.

CONCLUSIONS AND SIGNIFICANCE

Pulse response curves are measured in fresh NaMgA-zeolitic adsorbents; with the Henry constants and diffusion coefficients determined for i-butane, which does not enter the micropores, the response curves are calculated accurately in the time domain using a monodisperse pore model. Hydrothermally treated samples show a decrease in Henry constant and diffusivity as well as a large increase in skew. Using the parameter values determined from the first two moments, curve fitting is poor with the monodisperse model.

With the bidisperse macropore model described in this paper, the standard deviation of the calculated from the measured response curves is reduced tenfold. The fraction of damaged pores and the diffusional resistance term for both pore systems agree well at the three flowrates studied. However, apparently slight errors in the experimentally determined first moments lead to a dependency of the Henry constant and with it the diffusional time constant of the damaged pores on the flowrate. Plant efficiency with spent adsorbent charges such as we have studied would decrease much more sharply than predicted purely on the basis of the reduced overall parameter values.

ISSN 0001-1541-82-5216-0177-$2.00. © The American Institute of Chemical Engineers, 1982.

MATHEMATICAL ANALYSIS

In an earlier paper, Giddings (1963) recognized the significance of strongly skewed chromatographic response curves. However, the model he proposed considers only physical adsorption and desorption as rate-limiting steps. In recent years, following the work of Schneider and Smith (1968), it has become more common to consider the adsorption and desorption rate steps as extremely rapid, and to refer kinetic resistance to axial dispersion, external and internal diffusion.

Nevertheless, Vidal-Madjar and Guiochon (1977) found the Giddings model to be useful in treating highly skewed curves for which the Gram-Charlier series was inadequate. Chou and Hedegus (1978) noted that response curves obtained with spent catalysts could not be simulated on the basis of a monodisperse pore structure. They considered the outer shell of the spent catalyst to be a partially plugged layer, and calculated experimental curves accurately by taking into account diffusion through the outer layer and the inner region of the catalyst. However, they neglected adsorption in both zones of the porous media.

Our estimates below show that this approach would not be successful for systems of our type. While this manuscript was in preparation, Beekman and Froment (1979) calculated the aging

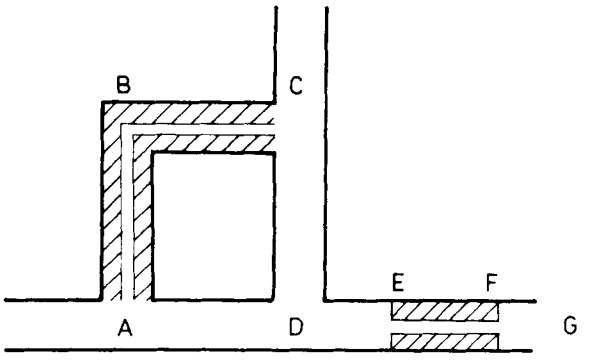

Figure 1. Schematic of pore structure in spent charge: *ABC, EF* = blocked pores.

kinetic of coked catalysts (but not their chromatographic response curves) on the basis of a statistical distribution of plugged pores, a concept similar to ours.

This investigation has been stimulated by chromatographic curves observed with a charge of hydrothermally treated NaMgA zeolites. Breck (1974) has discussed in some detail the effects of high-temperature steam treatment on A-zeolites, and in particular has shown that compacted samples deteriorate more rapidly than crystalline powders. We will consider the deposition of water-soluble materials in the macropores to be comparable to coke deposit in the macropores of catalysts. For this reason, the hydrothermally treated zeolite will be referred to simply as a "spent" charge below, and it is believed that the model may be applied to catalytic materials as well.

The macropore structure according to our model is shown in Figure 1. The pores AD and CD have averaged diameters and Henry constants for the unobstructed region of the pellet, whereas the pore ABC is plugged, increasing diffusional resistance, and the active adsorption centers have been covered by plugging material, reducing the Henry constant. The plugged pore ABC is roughly parallel to the path ADC, reducing the total porosity of the undamaged system, whereas the plugged pore EF is a series contribution, reducing the path length of the undamaged pores. The plugged pores are distributed stochastically throughout a network of unobstructed pores. Since the undamaged pores have a much lower diffusional resistance, they act as transport pores for the plugged regions.

The mass balance in the gas phase is:

$$D_{ax}\frac{\partial^2 c}{\partial x^2} - w\frac{\partial c}{\partial x} - \frac{3}{R_1}\frac{1-\epsilon}{\epsilon}D_{c1}\frac{\partial c_1}{\partial r_1}\bigg| = \frac{\partial c}{\partial t} \tag{1}$$

with the initial and boundary conditions for an impulse input,

$$i.c.\ c|_{t=0} = 0 \tag{2}$$

$$b.c.\ c|_{x=0} = c_\Delta \cdot t_0 \cdot \delta(t) \lim_{x\to\infty} c(t_1 x) = 0 \tag{3,4}$$

$c_\Delta \cdot t_o$ is the zeroth moment, the impulse is ideally represented by the Dirac distribution δ.

For the unobstructed region,

$$D_{c1}\left(\frac{\partial^2 c_1}{\partial r_1^2} + \frac{2}{r_1}\frac{\partial c_1}{\partial r_1}\right) - \frac{3}{R_2}\phi\,\beta a D_{c2}\frac{\partial c_2}{\partial r_2}\bigg|_{r_2=R_2} = (1-\phi)\beta_a\left(\frac{\partial c_1}{\partial t} + \frac{\partial q_1}{\partial t}\right) \tag{5}$$

with

$$i.c.\ c_1|_{t=0} = 0 \tag{6}$$

$$b.c.\ \frac{\partial c_1}{\partial r_1}\bigg| = 0 \qquad D_{c1}\frac{\partial c_1}{\partial r_1}\bigg| = k_f(c - c_1|) \tag{7,8}$$

and for the plugged pores

$$D_{c2}\left(\frac{\partial^2 c_2}{\partial r_2^2} + \frac{2}{r_2}\frac{\partial c_2}{\partial r_2}\right) = \phi\beta a\left(\frac{\partial c_2}{\partial t} + \frac{\partial q_2}{\partial t}\right) \tag{9}$$

TABLE 1. EQUIVALENCE OF NOTATION OF HAYNES (1975) AND THIS PAPER

Haynes	This Paper
θ_y	$(1-\phi)\beta_a$
K_a	K_{a2}
K_y	K_{a1}
D_z	$D_{ax}\cdot\epsilon$
D_y	D_{c1}
θ_z	ϵ
$\theta_x(1-\theta_y)$	$\phi\cdot\beta_a$
R_y	R_1
R_x	R_2
$D_x(1-\theta_y)$	D_{c2}

with

$$i.c.\quad c_2|_{t=0} = 0 \tag{10}$$

$$b.c.\quad \frac{\partial c_2}{\partial r_2}\bigg|_{r_2=0} = 0 \qquad c_2|_{r_2=R_2} = c_1 \tag{11,12}$$

In deriving Eqs. 5 and 9, it was assumed that the isotherms are linear

$$q_i = Kai\,Ci \quad (i = 1,2) \tag{13}$$

and that

$$D_{ci} = D_{\text{mod}}\,i\,\beta ai/\zeta_i^2 \quad (i = fr, 1,2) \tag{14}$$

where $D_{\text{mod},i}$ is the diffusion coefficient in a pore of averaged diameter. Equation 9 implies that the adsorbent sphere contains spherical inclusions with properties different from those of the sphere proper; the inclusions are small and numerous and uniformly distributed so that the model is formulated in terms of differential equations. Diffusion in randomly blocked pores would more properly be described in terms of plane geometry. We believe the blocked-pore conception, Figure 1, to be more probable than the spherical-inclusion model, but the quality of fits obtained will not depend greatly on the exact form of the diffusion terms (Ulin, 1974).

Equation 9 has been chosen because it permits use of bidisperse pore-structure routines, which should be available in many laboratories. We solved the system of differential equations by numerical inversion of the Laplace transformed solution according to Haynes (1975), as discussed by Friedrich et al. (1979). In adapting the Haynes solution to our problem we rewrote his Eq. 20 as:

$$C = \left\{\frac{\theta_y(1+K_y)N_1}{N_3}S + 3(1-\theta_y)N_4(D\coth D - 1)\right\}^{1/2} \tag{15}$$

to account for adsorption in the transport pores. The resulting solution describes the output curve $y(t)$, with

$$y = \frac{c}{c_0};\quad c_0 = \frac{W}{X}\mu_{0|\text{emp}} \tag{16}$$

The normalization factor c_0 is chosen so that the zeroth moment equals unity.

The moments of Eqs. 1-13 are:

$$\mu_1^1 = \frac{X}{w}(1 + m\kappa_{\text{emp}}) \tag{17}$$

$$\mu_2 = \frac{2X}{w}\left[\frac{D_{ax}}{w^2}(1+m\kappa_{\text{emp}})^2 + m\kappa_{\text{emp}}^2\left\{\frac{R_0}{3k_f} + \frac{R_1^2}{15D_{c1}}\right) + m\kappa_2^2\cdot\frac{R_2^2}{15\,D_{c2}}\right] \tag{18}$$

with

$$\kappa_{\text{emp}} = \kappa_1 = \beta_a(1 + K_{a|\text{emp}}) = \beta_a + (1-\phi)\beta_a K_{a1} + \phi\beta_a K_{a2} \tag{19}$$

and

$$\kappa_2 = \phi\beta_a(1 + K_{a2}) \tag{20}$$

From the experimental first moment and Eq. 17, κ_{emp} may be determined. Further evaluation requires independent estimation of D_{ax} and k_f. The reduced second moment is defined as:

$$\eta = \frac{\mu_2}{2(\mu_1')^2} = \frac{2R_0}{Pe_\infty X} + \frac{w}{X}\left[\left(\frac{m\kappa e_{emp}}{1 + m\kappa_{emp}}\right)^2\left(\frac{R_0}{3k_{fm}} + \frac{R_1^2}{15\,D_{c1m}}\right) + \left(\frac{m\kappa_2}{1 + m\kappa_{emp}}\right)^2\frac{R_2^2}{15\,D_{c2m}}\right] \tag{21}$$

Plotting ηX vs. w gives a straight line at higher velocities, where the equation:

$$D_{ax} = 0.7\,D_{AB} + \frac{2R_0 w/Pe_\infty}{1 + 7\,D_{AB}/2R_0 w} \tag{22a}$$

simplifies to

$$D_{ax} = 2\,R_0 w/Pe_\infty \tag{22b}$$

Equation 22b has been substituted into Eq. 21. The intercept of the straight line with the ordinate axis determines Pe_∞, which may then be entered into Eq. 22a to calculate D_{ax} as a function of the flowrate. Laminar boundary layer coefficients k_f were estimated according to Bird et al. (1966). If K_{a1} is known and K_{a2} and R_1^2/D_{c1} have been guessed, rearranging Eqs. 18 and 19:

$$\phi = (K_{a1} - K_{a1emp})/(K_{a1} - K_{a2}) \tag{23}$$

and

$$\frac{R_2^2}{D_{c2}} = \frac{15}{m\kappa_2^2}\left[\frac{w\mu_{2,emp}}{2X} - \frac{D_{ax}}{w^2}(1 + m\kappa_{emp})^2 - m\kappa_{emp}^2 \times \left(\frac{R_0}{3k_f} + \frac{R_1^2}{15\,D_{c1}}\right)\right] \tag{24}$$

so that all parameters have been determined. The output curve may now be calculated and the standard deviation from the experimental curve σ obtained.

When treating the adsorbents as a monodisperse system, R_2^2/D_{c2} and K_{a1} are equal to zero and $\phi = 1$. Using the Haynes, Jr. program, the former was accomplished by setting N_4 equal to 10^6.

A comparison of our model with the Chou-Hegedus theory (corrected for adsorption capacities) has been made on the basis of the calculated skew:

$$S = \mu_3/\mu_2^{3/2} \tag{25}$$

Neglecting axial dispersion and boundary-layer resistance contributions, the third moment is estimated as:

$$\mu_3 = 12 \times m\,\zeta/w \tag{26}$$

with

$$\xi = \frac{5}{7}\kappa_{emp}^3\left(\frac{R_1^2}{15\,D_{c1}}\right)^2 + \frac{5}{7}\kappa_2^3\left[\frac{R_2^2}{15\,D_{c2}}\right]^2 + \kappa_{emp}\,\kappa_2^2 \cdot \frac{R_1^2}{15\,D_{c1}} \cdot \frac{R_2^2}{15\,D_{c2}} \tag{27}$$

The difference in skews calculated by the two models may be understood on the basis of the results in Table 2, using typical input data for our case over a range of ϕ; the lowest possible ϕ is 0.64 for $K_{aj} = 0$. If the spent region is distributed along the transport pores ($j = 2$), then $K_{a2} \ll K_{a1}$, and $\kappa_2 \ll \kappa_{emp}$, column 2. According to Eq. 24, R_2^2/D_{c2} (column 4) varies inversely proportional to κ_2^2, leading to a large ξ (column 6), since the second term on the right-hand side of Eq. 27 dominates.

If the spent region is the outer shell ($j = 1$, columns 3, 5, 7), then $K_{a1} \ll K_{a2}$, and κ_{emp} and κ_2 are of the same order of magnitude, so that ξ remains small. Table 2 shows that ξ and thus the skew of our model may be varied thirty-five fold, whereas that of the outer-shell model only by 15%. This is the quantitative expression of our model conception that a relatively small fraction of tracer enters the plugged zone, which has a high resistivity, leading to the pronounced tailing.

TABLE 2. COMPARISON OF SKEWS WITH DIFFERENT MODELS
1 = outer region, 2 = inner region
i = undamaged region, j = plugged region
$K_{ai} = 30$, $R_i^2/D_{ci} = 6.08$, $\kappa_{emp} = 3.885$

	κ_2		R_j^2/D_{cj}		ξ	
ϕ_j	$j = 2$	$j = 1$	$j = 2$	$j = 1$	$j = 2$	$j = 1$
0.64	0.05	3.78	60,960	13.3	1,488	44
0.7	0.63	3.15	384	14.4	139	46
0.8	1.7	2.10	52	15.5	67	47
0.9	2.8	1.05	19	16.1	37	49

It should be noted that others, including Haynes, Jr. (1975) have calculated families of response curves with increasing skew, but in doing so varied both the second and third moments. The problem here is to calculate a highly-skewed response curve with a given experimental value of the second moment.

Experimental Studies

Experimental work was carried out in equipment which has been described before (Wolff et al., 1980). The chromatographic column was packed with various charges of compacted zeolite NaMgA, with a window opening of 0.5 nm. Use of iso-butane as tracer, which does not fit through the window, permitted selective investigation of the macropore structure. Air served as carrier gas, the temperature was 348 K, pressure was normal, and pressure drop less than 0.1 of the outlet pressure.

Results were monitored by a process computer, which triggered the pulsing valve at the start of a run, determined the end of the run independently, calculated and printed the first three moments, and then triggered the next run until the desired number of repetitions under identical conditions had been obtained. In this manner, routine analysis of a large number of charges was rapidly performed, moments evaluation being based on some 20 peaks at each of up to ten different velocities.

On special order, the routine could be interrupted and concentration-time data printed for purposes of recalculating the response curve with the parameters determined. Output data were stored at a rate chosen to utilise maximum storage capacity in the process computer, so that some 800 concentration values were available for each curve when computing the moments. Since curve-fitting in the time domain was performed with concentrations selected at equidistant steps along the time scale, n, Eq. 31 below, increased from 26 to 52 with decreasing flowrate. Agreement between model and measured curves had been so good for all (fresh) samples previously measured, that the possible significance of curve-fitting with the spent charge considered in this work was not recognised until the series of runs was completed and the charge discarded. Thus, only one curve at each of three flowrates is available for this study.

Further, we have no definite information as to which of the fresh charges was the initial material for the spent charge. Under these conditions we may not claim to offer final proof of the physical reality of our model applied to the charge studied. On the other hand, the three individual curves are typical of the twenty repetitions at each flowrate. Individual moments vary from the average of a species of twenty by a maximum of 0.4% in the first moment, 2.6% in the second moment and 7.7% in the third moment; these errors lie within the standard deviation limits. The individual moments are neither consistently higher nor lower than the average vlaues, and no individual curve at any flowrate has the largest deviation from the average in all three moments.

The first moments of the spent charge, Figure 2, Curve 1, are considerably lower than those for a typical fresh charge, Curve 2. Henry constants for the spent charge using the monodisperse model are about 10, whereas the average value for a fresh charge of similar binder composition and content equals about 30. Both curves in Figure 2 deviate to some degree from the expected linearity, the points at higher reciprocal flowrates falling below the line determined by the method of least squares. Tests with varying tracer concentration confirmed this trend, but the Henry constant was independent of tracer concentration. Therefore, deviations from Henry's law would not appear to be the cause. The straight lines in Figure 2 have been fitted through the origin; better agreement with the first moments over the range of flowrates is obtained when an ordinate intercept is allowed for. However, the statistically determined intercept with the spent charge was 8 s, a value too large to be reasonably considered as a "dead time" in the column entrance or sampling lines. Some other source of error must be found if this effect is to be eliminated.

Agreement with the linear form of Eq. 21 for the reduced second moments is much better, Figure 3, where only scatter is recognised over the entire range of velocities. Since η is the ratio of two moments, it may be

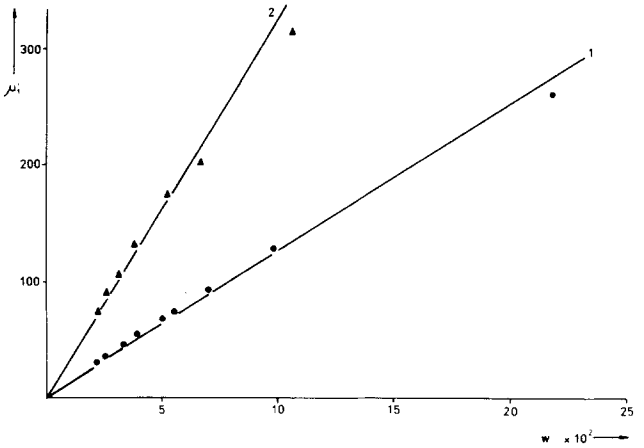

Figure 2. First moments vs. reciprocal flowrate: ▲ fresh charge, ● spent charge.

concluded that errors in the moments are compensating when evaluation is carried out by Eq. 21. The higher slope for the spent charge, Curve 1, leads to an effective diffusion coefficient of 1.3×10^{-3} [$cm^2 \cdot s^{-1}$] according to the monodisperse model, whereas for the fresh charge an average value of 3.7×10^{-3} [$cm^2 \cdot s^{-1}$] is found.

Although the reduction of the Henry constant and the diffusivity of the spent charge by about two-thirds is a significant result, the difference in curve-fitting with the monodisperse model is more spectacular. The fresh sample yields excellent agreement with the experimental response curves in Figure 4. Standard deviations are 0.0020 and 0.0018, using the constants determined on the basis of the first two moments of the individual curves.

This testifies to the high quality of the experimental and recording equipment, and indicates that deviations recognised in Figure 2 are of no great importance in this case. In Figure 5, the skew is plotted as a function of the first moment, where the curves have been drawn free-hand. We have observed that experimental skews such as those of the fresh charge, Curve 2, are typical of response curves which may be simulated by the monodisperse model, whereas the larger skews of the spent charge, Curve 1, are not approached by the monodisperse model. Thus, there is no satisfactory agreement for the spent sample, Figure 6, in which the monodisperse curve-fitting is shown by the dashed lines. Standard deviations (Table 3) are 25 times larger than those of the fresh sample.

The high skew of the curves is not just reflected in the pronounced tail. The curve-fitting procedure described below involves minimisation of squared deviations, and the deviation in the tail is small since the experimental values themselves are small. The high skew is reflected in an increase in the maximum value of the response curve and a sharpening of the curve in the vicinity of the maximum, Figure 6. This is the region having the most pronounced effect on curve fitting and accounts for the need of a model yielding high skew, although we did not optimise the calculated skew value. Agreement of the first three moments with the experimental values is indeed an insufficient criterion, since a larger number of moments is needed for a satisfactory description of the response curve using for example the Hermite polynomials (Wiedemann et al., 1978).

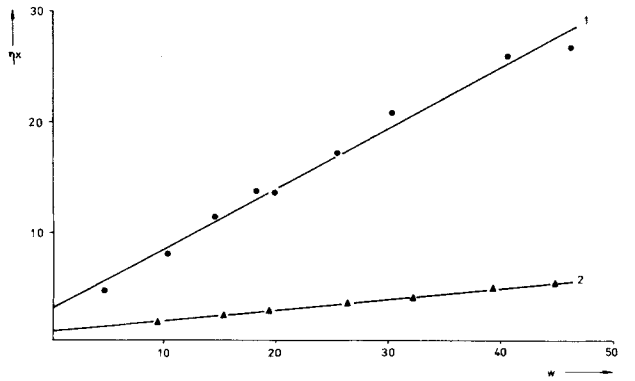

Figure 3. Reduced second moment vs. flowrate: ▲ fresh charge, ● spent charge.

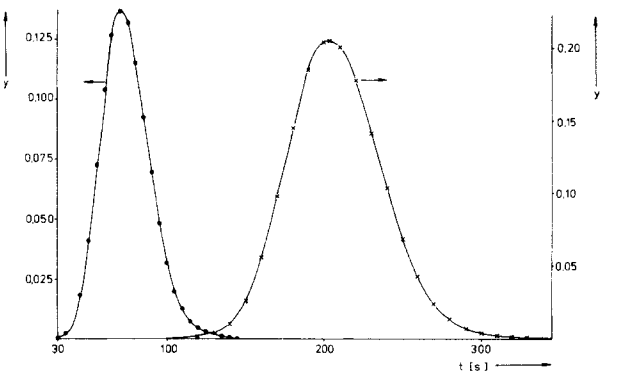

Figure 4. Curve Fitting for fresh charge: ● 44.7 cm.s^{-1}, X 15.22 cm.$^{-1}$, — monodisperse model.

In curve-fitting the spent charge with our model, we assumed that K_{a1} equals 30, the average value of the fresh charges. However, the diffusivity may not be assumed equal to the fresh value. Since

$$D_{c1} = Dc_{1fr} \cdot \frac{D_{\mathrm{mod},1}}{D_{\mathrm{mod},fr}} \cdot \frac{\beta_{a1}}{\beta_{a,fr}} \cdot \frac{\zeta_{fr}^2}{\zeta_1^2} \tag{28}$$

and both β_a and ζ_1 are influenced by pore blockage, it is not possible to differentiate amongst the factors on the right-hand side of Eq. 28. Therefore, the diffusional time constants:

$$\tau_i = R_i^2/D_{ci} \quad (i = 1,2) \tag{29}$$

will be considered below. The τ_i do not enter directly into the second moment, Eq. 18, but rather the total resistance terms ρ_i,

$$\rho i = \kappa_i^2 \, \tau_i/15 \quad (i = 1,2) \tag{30}$$

The ρ_i depend on the κ_i defined by Eqs. 19 and 20.

Using a two-parameter search procedure, computer input values of K_{a2} were varied for a series of τ_1 at each flowrate. The ϕ and τ_2 were determined from Eqs. 23 and 24, the output curve $y_{\mathrm{mod}}(t)$ was calculated by the Haynes procedure and the standard deviation given by:

$$\sigma = \left\{\frac{1}{n}\sum(y_{\mathrm{mod}} - y_{\mathrm{emp}})^2\right\}^{1/2} \tag{31}$$

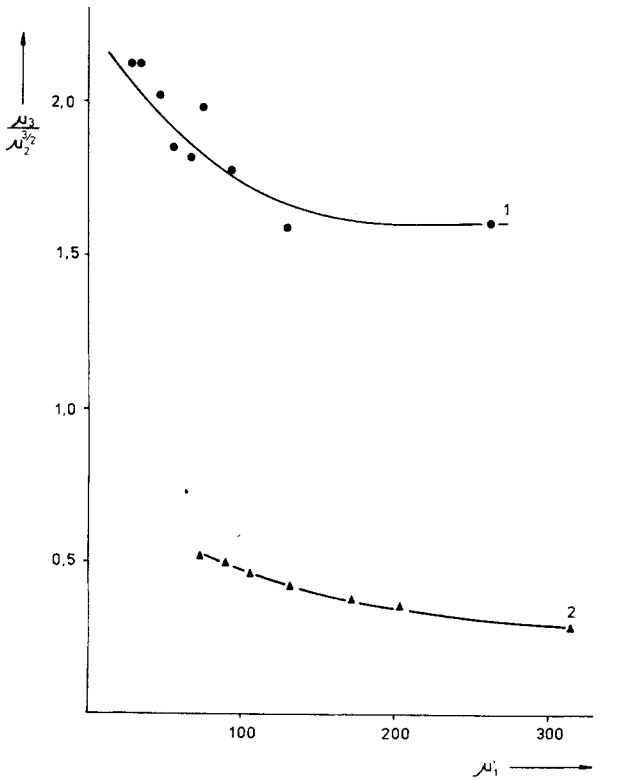

Figure 5. Skew vs. first moment: ▲ fresh charge, ● spent charge.

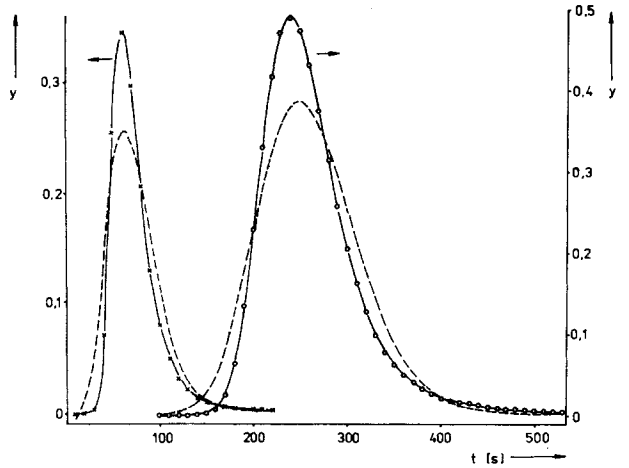

Figure 6. Curve fitting for spent charge: X 18.2 cm.s^{-1}, O 4.6 cm.s^{-1}, - - - monodisperse model, —— our model.

For each τ_1 and w, σ was plotted as a function of K_{a2}, yielding a local minimum σ_{min}. The global minimum standard deviation over all K_{a2}, τ_1 is defined as σ_{opt}. Step sizes in input data were 0.5 for K_{a2} and 0.5 s in τ_1; graphical interpolation was performed within these limits. After a few runs the number of K_{a2}-variations at each τ_1 could be readily restricted to the range yielding the local minimum.

Optimum curve fitting is shown as full lines in Figure 6 at two of the three flowrates; the symbols are the experimental points. Curve fitting is highly satisfactory in all cases and standard deviations are reduced sharply (See below.)

A far more stringent test of model adequacy consists in comparing optimum parameters at the three flowrates. Chou and Hegedus (1978) made no such study, presenting experimental data at only one flowrate. In our case, parameters at the three flowrates agree well with some reservations.

Model 1 in Table 3 is the monodisperse approach. The overall Henry constant $K_{a,emp}$ increases with flowrate, reflecting the curvature in Figure 2. The time constant τ_{emp} decreases with flowrate, but the resistance term ρ_{emp} only scatters about the average value of 15.3 s with a maximum error of about 10%. The agreement among second moments is thus very good, whilst the apparent dependency of the time constants on the flowrate is a direct result of evaluation with increasing Henry constants. Despite the good agreement among resistance terms at all flowrates, curve fitting is poor and standard deviation σ is high.

Optimization with our model, Model 2, yields an almost constant fraction of damaged pores ϕ at all flowrates. The τ_1 are equal at the two higher flowrates whereas the value at the lowest flowrate appear to small. However, the resistance of the undamaged region was only ten to twenty percent of the total diffusional resistance, so conditions were not favorable for determining τ_1. Further, σ_{opt} was not very sensitive to τ_1, so that near-optimum deviations will be obtained below with constant τ_1.

The optimum K_{a2} increase with flowrate, but this may be traced directly to the increase in $K_{a,emp}$, aggravated by the subtraction involved in Eq 23; the τ_2 react accordingly. However, the ρ_2 are again independent of flowrate and scatter about the average value of 12.4 s with a maximum error of only 13%. Finally, the standard deviation is reduced by over 90% of the value obtained with the monodisperse model at all flowrates.

Closer inspection reveals a range of ρ_1 between 2.4 and 2.8 s within which all three response curves may be fitted to a standard deviation of less than 0.01. The last three rows in Table 3 list the near-optimum parameters. Standard deviation has been reduced by over 85% of the monodisperse values, ρ_1 is independent of flowrate and scatter among the ρ_2 is small.

The measured diffusion coefficient for the fresh charge $D_{c,fr}$ as given above is 3.7×10^{-3} [cm^2·s^{-1}]. The optimum value for the undamaged zone of the spent charge, based on $R_0 = 0.15$ [cm], is $D_{c1} = 6 \times 10^{-3}$ [cm^2·s^{-1}]. The local minimum standard deviation with $D_{c,fr}$ is two to three times greater at each of the three flowrates than the global minimum. Referring to Eq. 28, and taking into account the reduction in $\beta_{a1} = (1 - \phi)\beta_{a,0}$, the increase in D_{c1} may be explained by a sixfold reduction in the squared effective path length $R_0^2 \zeta_1^2$ or an equivalent increase in $D_{mod,1}$, or contributions of both.

A reduction in effective path length can be caused by pore segments such as *EF*, Figure 1, becoming part of the damaged zone. $D_{mod,1}$ could increase as a result of selective blockage of narrower pores. In a recent publication (Wolff and Gelbin, 1980) we discussed porosimetric measurements of these charges, which are Samples 1 and 2 of that paper. Total porosity is reduced from 0.5 to 0.35 [cm^3·cm^{-3}], but we found no quantitative relationship between pore-size distribution curves and the effective pore diameter determined by chromatographic measurements. No conclusions pertaining to the pore model proposed here can be drawn.

Summarizing, our model is capable of highly satisfactory curve fitting at all flowrates. The fraction of damaged pores, the diffusional resistance terms for both regions and the time constant of the undamaged pores agree well for all curves. However, the Henry constant and the time constant of the damaged pores vary with the overall Henry constant; future work must concentrate on eliminating the source of curvature in Figure 2.

This paper indicates that partial blockage of the macropores may cause the highly skewed chromatographic curves observed. The same differential equations apply to the simulation of breakthrough curves, substituting the Heaviside for the Dirac entrance boundary condition. With adsorbent charges such as we have studied, breakthrough curves in systems with macropore diffusion limiting would be smeared and plant separation efficiency would decrease to a degree well beyond that predicted purely on the basis of reduced overall macropore diffusivities and Henry constants.

TABLE 3. RESULTS OF CURVE FITTING

w	w_1 4.56	w_2 18.23	w_3 46.35
Model 1—Values from Experimental Moments			
$K_{a,emp}$	8.5	9.9	10.1
τ_{emp}	19.6	17.4	14.6
ρ_{emp}	14.4	16.9	14.7
$10^3\sigma$	84	52	48
Model 2—Optimum Values			
ϕ_2	0.75	0.74	0.76
τ_1	2.05	3.75	3.75
K_{a2}	1.0	3.0	4.0
τ_2	705	189	92
ρ_1	1.5	3.5	3.8
ρ_2	12.9	13.5	10.8
$10^3\sigma$	6.6	4.9	4.3
Model 2—Near Optimum Values			
ρ_1	2.8	2.8	2.8
ρ_2	11.6	14.1	11.9
$10^3\sigma$	10.0	7.8	7.2

NOTATION

c = concentration in the gas phase, mol/cm^3
c_o = normalization factor, mol/cm^3
c_Δ = tracer-concentration of the pulse, mol/cm^3
C = factor (see Haynes, 1975)
D = factor (see Haynes, 1975)
D_{AB} = molecular diffusivity, cm^2/s
D_{ax} = axial dispersion coefficient, cm^2/s
D_c = pore diffusion coefficient, cm^2/s
K_a = adsorption equilibrium constant
K_y = see table 1
k_f = laminar boundary layer coefficient, cm/s
m = geometric factor m = $(1 - \epsilon)/\epsilon$
n = number of values
N_1, N_3, N_4 = factors (see Haynes, 1975)
Pe_∞ = asymptotic Pe at high flowrates
q = adsorbed concentration, mol/cm^3
r = diffusional path length, cm
R = total radius, cm
s = Laplace transform variable, s^{-1}
S = skew coefficient of the response curve
t = time, s
t_o = pulse time, s
w = linear flowrate, cm/s
x = distance from bed inlet, cm
X = total height of bed, cm
y = reduced gas phase concentration

β_a = void fraction of porous solid
ϵ = void fraction of packed bed
η = reduced second moment
θ_y = see table 1
κ = capacity factor for tracer
$/u_0$ = zeroth moment
$/u'_1$ = first absolute moment, s
$/u_2$ = second central moment, s^2
$/u_3$ = third central moment, s^3
ξ = see Eq. 27
ρ = total resistance term, s
σ = standard deviation
τ = diffusional time constant, s
ϕ = fraction of plugged pores
ζ = tortuosity factor

Indices

0 = of the particle
1 = of the unobstructed region
2 = of the plugged regions
emp = empirical value
mod = model
min = minimal value
fr = of the fresh particles
opt = optimal value

LITERATURE CITED

Beeckman, J. W. and G. F. Froment, "Catalytic Deactivation by Active Site Coverage and Pore Blockage," *Ind. Eng. Chem. Fund.*, **18**, 245 (1979).

Bird, R. B., W. E. Stewart and E. N. Lightfoot, "Transport Phenomena," Havanna (1966).

Breck, D. W., "Zeolite Molecular Sieves," Chapter 6, John Wiley and Sons, New York-London-Sydney-Toronto (1974).

Chou, T.-S. and L. L. Hegedus, "Transient Diffusivity Measurements in Catalyst Pellets with Two Zones of Differing Diffusivities," *AIChE J.*, **24**, 255 (1978).

Friedrich, S., C. Bode and W. Flock, "Investigation of the diffusion in bidisperse structured catalysts by gas chromatography. A note on the time domain solution," *Chem. Eng. Sci.*, **34**, 418 (1979).

Giddings, J. C., "Kinetic Origin of Tailing in Chromatography," *Anal. Chem.*, **35**, 1999 (1963).

Haynes, Jr., H. W., "The Determination of Effective Diffusivity by Gas Chromatography. Time Domain Solution," *Chem. Eng. Sci.*, **30**, 955 (1975).

Kubin, M. "Beitrag zur Theorie der Chromatographie," *Coll. Czech. Chem. Commun.*, **30**, 1104 (1965).

Ruckenstein, E., A. S. Vaidyanathan and G. R. Youngquist, Sorption by solids with bidisperse pore structures," *Chem. Eng. Sci.*, **26**, 1305 (1971).

Schneider, P. and J. M. Smith, "Adsorption Rate Constants from Chromatography," *AIChE J.*, **14**, 762 (1968).

Ulin, W. I., "Determining diffusion coefficients in bidisperse cylindrical adsorbent particles," Russian, *Izv. akad. nauk*, USSR, ser. chim. 2148 (1974).

Vidal-Madjar, C. and G. Guiochon, "Experimental Characterisation of Elution Profiles in Gas Chromatography," *J. of Chromatography*, **142**, 61 (1977).

Wiedemann, K., A. Roethe, K.-H. Radeke and D. Gelbin, "The Modelling of Adsorption-Desorption Breakthrough Curves Using Statistical Moments," *The Chem. Eng. J.*, **16**, 19 (1978).

Wolff, H.-J., K.-H. Radeke and D. Gelbin, "Weighted Moments and the Pore Diffusion Model," *Chem. Eng. Sci.*, **35**, 1481 (1980).

Wolff, H.-J. and D. Gelbin, "Makroporenmodelle und Tortuositätsfaktoren in porösen Festkörpern," *Chem. Technik*, **32**, 362 (1980).

Manuscript received June 9, 1980; revision received April 6, and accepted April 23, 1981.

An Analysis of Bacterial Growth in Fluidized-Bed Adsorption Column

An analysis is presented to describe the dynamics of fluidized bed adsorption columns. A microbial film model (recently proposed by the authors) is used to characterize the bacterial activity and its interaction with adsorption and solids mixing. Solids mixing and mixing in the liquid phase are included in the analysis, as is the effect of microbial film growth on the settling velocity of the adsorbent particles. The interplay of film growth, bed stratification and solids mixing is discussed in detail.

G. F. ANDREWS and CHI TIEN

Department of Chemical Engineering and Materials Science
Syracuse University, Syracuse, NY 13210

SCOPE

It is known that bacterial films may develop on the surface of activated carbon particles in adsorption columns treating biodegradable wastewaters. The films have some beneficial effects, including direct uptake of organic matter from the waste stream and "bioregeneration" of the carbon. Because of these effects, fluidized-bed columns in which bacterial growth is encouraged have been proposed as combined bacteria/carbon treatment units. However, there are also deleterious effects such as the extra mass-transfer resistance that the film presents to adsorption.

This paper gives a mathematical model that can be used to include all these effects in the design of adsorption columns, and to evaluate various schemes for fluidized-bed, bacteria/carbon treatment units. This is the first published model to incorporate uncontrolled active bacterial growth. The resulting thick films not only cause bioregeneration but also alter the settling velocity of the carbon particles. This leads to a varying bed height, a

G. F. Andrews is presently with the Deparument of Chemical Engineering, State University of New York at Buffalo, Amherst, NY 14260.

ISSN 0001-1541-82-5217-0182-$2.00.

© The American Institute of Chemical Engineers, 1982.